JOURNAL OF MATERIALS SCIENCE 33 (1998) 3875–3884

Early fatigue damage in carbon-fibre composites observed by electrical resistance measurement

S. WANG, X. SHUI, X. FU, D. D. L. CHUNG
Composite Materials Research Laboratory, State University of New York at Buffalo, Buffalo, NY 14260-4400, USA
E-mail: ddlchung@acsu.buffalo.edu

Early fatigue damage during the first tenth (or less) of the fatigue life was observed in carbon fibre composites by d.c. electrical resistance measurement. The damage was most severe in the first loading cycle and the incremental damage in each subsequent cycle diminished cycle by cycle. For the continuous carbon fibre carbon-matrix composite, the resistance increased irreversibly during early fatigue due to matrix damage and possibly fibre fracture as well. For the short carbon fibre polymer-matrix and cement-matrix composities, the resistance decreased irreversibly during early fatigue due to matrix damage near the junction of adjacent fibres and the resulting increase in the chance that adjacent fibres touched one another.

Introduction

Fatigue is one of the most common causes of failure of structures, as most structures encounter dynamic loading. The study of fatigue has been concentrated at the end of the fatigue life rather than over the entire fatigue life, as determination of the fatigue life dominates fatigue studies and this determination requires attention mostly near the end of the fatigue life. However, understanding the fatigue process requires investigation of the entire evolution of fatigue damage. For this purpose, the extent of damage needs to be monitored throughout the fatigue life. Owing to the extensive nature of damage shortly before fatigue failure, the sensing of fatigue damage near the end of fatigue life is not difficult. For example, it can be achieved by acoustic emission measurement. However, the sensing of early fatigue damage is relatively difficult, because early damage is not as extensive as the damage near the end of the fatigue life. In spite of the difficulty of detecting early fatigue damage, this detection is important in practice for hazard mitigation and lifetime prediction, and is scientifically valuable for understanding the mechanism of fatigue. By monitoring fatigue by electrical resistance measurement, we have been able to observe damage as early as the first cycle of loading. This early damage is most severe in the first cycle and the incremental damage in each subsequent cycle diminishes cycle by cycle until the incremental damage per cycle approaches zero. This early damage regime occupies the initial small fraction (<10%) of the entire fatigue life.

There exist several methods to monitor fatigue damage. The acoustic emission (AE) technique has been used for this purpose [1–3] and for monitoring other kinds of damage [4–6] since the 1970s. It is non-invasive to the material being monitored, and can give us information about fracture mechanisms, etc. However, AE needs relatively complicated equipment, and can be influenced by external noises. The fibre-optic sensing technique is also a popular method [7]; it is sensitive but somewhat invasive. Electrical resistance measurement is a less common method [8–10]; the benefit of this technique is associated with its simple use and accuracy [11]. Moreover, it is non-invasive, can sense the whole volume of the material, and is more sensitive to the early stage of damage.

The use of electrical resistance measurement to monitor damage is based on the notion that damage causes the electrical resistivity to change irreversibly, in contrast to elastic strain, which causes the resistance (and possibly the resistivity as well) to change reversibly. For example, cracks would cause the resistivity to increase. A benefit of the electrical resistance measurement is that it provides information on the dynamic strain through the reversible resistance change, in addition to information on the damage through the irreversible resistance change. Thus, both strain and damage are sensed in real-time during fatigue. The combined ability to monitor both reversible strain and damage is particularly valuable in real-time fatigue damage monitoring under dynamic loading which may or may not be periodic in time, because the strain cycle and the point within the cycle at which damage occurs can be identified. The dynamic strain-sensing ability is essentially absent in acoustic emission measurement.

A structure experiences dynamic strain during use. The monitoring of the strain is useful for control of

0022–2461

the structure, in order to make the structure "smart". Embedded or attached strain sensors are conventionally used for the strain monitoring. These sensors can be optical fibre and a variety of strain gauges. They suffer from poor durability and, in the case of embedded sensors, they have the tendency to degrade the mechanical properties of the structure. In contrast, in this work we have employed a carbon fibre composite itself as the strain sensor to monitor the composite's own strain (i.e. to self-monitor the strain), based on the reversible increase of the electrical resistance upon straining. In addition, the composite monitors its own damage.

This paper describes the use of electrical resistance measurement to monitor fatigue damage in carbon fibre composites, namely continuous carbon fibre carbon-matrix composite (or carbon–carbon composite) [12], short carbon fibre polymer-matrix composite [13] and short carbon fibre cement-matrix composite [14]. Carbon is suitable for this method because it is electrically conducting. Moreover, carbon fibre composites are technologically important for aerospace, automobile, marine, construction, machinery, biomedical and other applications.

2. Carbon–carbon composite

Carbon–carbon composites with continuous carbon fibres are used for high-temperature aerospace structures, due to the high-temperature resistance of the carbon matrix in these composites. The carbon matrix, though much more high-temperature resistant than a polymer matrix, is much more brittle than a polymer matrix. This brittleness makes carbon–carbon composites prone to matrix cracking. As a result, there is a need for monitoring the condition or health of a carbon–carbon composite structure while the structure is in use.

2.1. Experimental procedure

The carbon–carbon composite, kindly provided by Sigri Great Lakes Carbon Corp. (Union, NJ) under the grade designation of CC 1501G, was in the form of a sheet containing carbon fibre roving fabric (90° biaxial weaving) and was produced by lamination and compression. The heat-treatment temperature used in production was 2000 °C. According to the manufacturer, the bulk density was 1.40–1.45 g cm^{-3}, the open porosity was 20%–25%, the bending strength was 210–250 MPa, the dynamic modulus of electricity was 60–65 GPa, the interlaminar shear strength was 9–12 MPa and the ash content was 0.08%. According to our measurement, the tensile strength was ~382 MPa.

The electrical resistance, R, was measured in the direction of one of the two perpendicular sets of fibres using the four-probe method, while cyclic and static tension until failure was applied in the same direction. Silver electrically conducting paint was used for all electrical contacts. The four probes consisted of two outer current probes and two inner voltage probes. The resistance, R, refers to the sample d.c. resistance between the inner probes. The four electrical contacts were placed around the whole perimeter of the sample in four parallel planes that were perpendicular to the stress axis, such that the inner probes were 60 mm apart. The specimen was of length 85 mm, width 6.80 mm and thickness 2.46 mm. The stress axis was along the longest dimension of the specimen. One strain gauge was attached to the centre of one of the large surfaces of a specimen to measure the strain in the longitudinal direction. Two strain gauges were attached to the centres of the two opposite large surfaces of a specimen to measure the strain in the transverse direction. Two other strain gauges were attached to the two opposite small surfaces to measure the strain in the thickness direction. The strains from each pair of strain gauges were averaged. The average strains were used to calculate Poisson's ratios in the transverse and thickness directions, ν_{12} and ν_{13}, respectively. A Keithley 2001 multimeter and a hydraulic mechanical testing system (MTS 810) were used.

2.2. Results and discussion

Fig. 1 shows the stress (curve a) and the fractional resistance increase, $\Delta R/R_0$ (curve b) obtained during static tension up to failure. $\Delta R/R_0$ increased monotonically with strain, such that the increase was gradual (only slightly above the increase in $\Delta R/R_0$ due to the changes in dimensions, curve (c) in Fig. 1) at low strains and abrupt at high strains.

Fig. 2 shows $\Delta R/R_0$ obtained during cyclic tension to a stress amplitude (360 MPa) equal to 94% breaking stress. The tensile strain was almost totally reversible. The irreversible strain was 0.040% at the end of the first cycle, and increased very slightly with increasing cycle number. $\Delta R/R_0$ increased upon loading in every cycle, such that it irreversibly increased slightly after every cycle and the irreversible increase in $\Delta R/R_0$ was particularly large for the first cycle, as shown in Fig. 2. At fatigue failure, $\Delta R/R_0$ abruptly increased, such that $\Delta R/R_0$ no longer rapidly increased irreversibly near the end of fatigue life. Fig. 3 shows the peak $\Delta R/R_0$ values in a cycle as a function of cycle number throughout the fatigue life up to failure. The peak $\Delta R/R_0$ increased significantly with cycle number

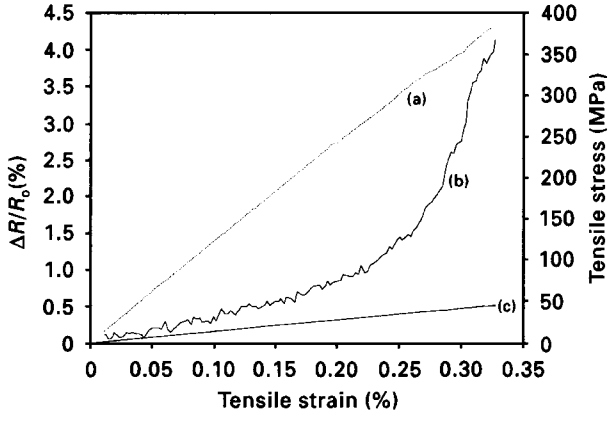

Figure 1 Plots of (a) tensile stress versus strain, and (b) $\Delta R/R_0$ versus strain, obtained simultaneously during static tension up to failure for a carbon–carbon composite. (c) The calculated $\Delta R/R_0$ based on dimensional changes.

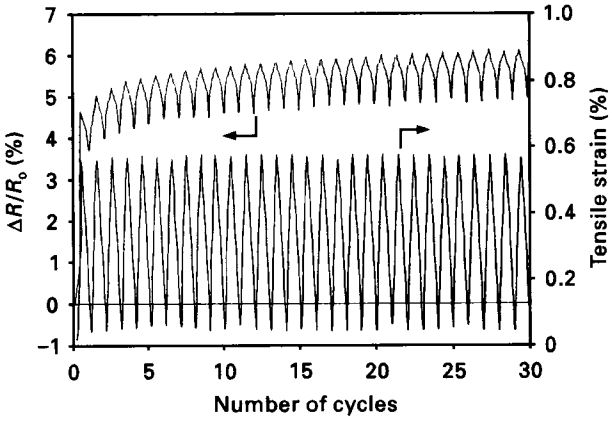

Figure 2 Plots of $\Delta R/R_0$ versus cycle numbers and of tensile strain versus cycle numbers obtained simultaneously during first cyclic tension of a carbon–carbon composite at a stress amplitude of 94% fracture stress.

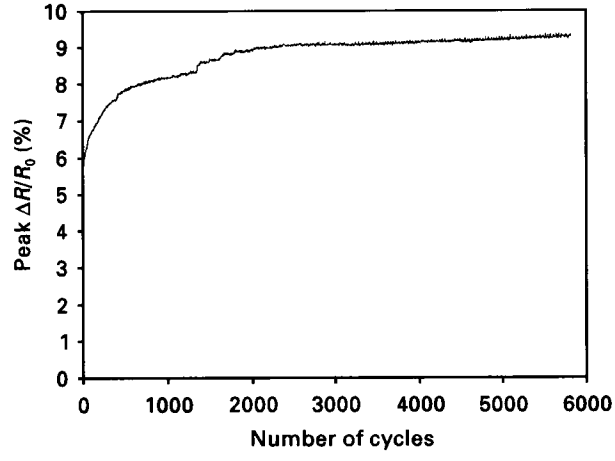

Figure 3 Variation of the peak $\Delta R/R_0$ with cycle numbers throughout the entire fatigue life at a stress amplitude of 94% fracture stress for a carbon–carbon composite.

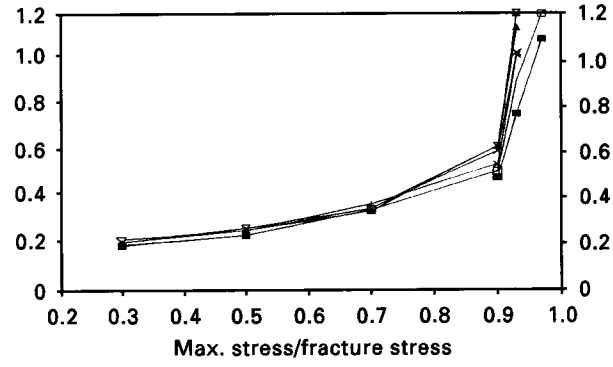

Figure 4 Variation of the reversible part of $\Delta R/R_0$ with stress amplitude (fraction of fracture stress) for various fixed cycle numbers ((■) 1, (□) 20, (✳) 100, (×) 200, (▲) 300 and (⧖) 2000) for a carbon–carbon composite.

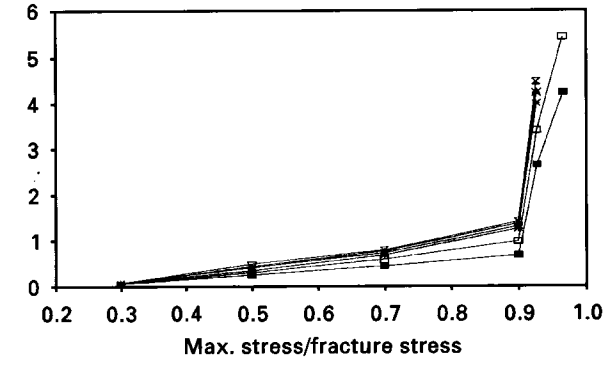

Figure 5 Variation of the irreversible part of $\Delta R/R_0$ with stress amplitude (fraction of fracture stress) for various fixed cycle numbers ((■) 1, (□) 20, (✳) 100, (×) 200, (▲) 300 and (⧖) 2000) for a carbon–carbon composite.

during the first 500 cycles and gradually during all subsequent cycles up to failure. The small step increases in the peak $\Delta R/R_0$, for example at ~1350 cycles, are not experimental artifacts but are attributed to damage occuring at those cycle numbers, similar to the step increases observed for a continuous carbon fibre polymer-matrix composite under similar cyclic loading [15].

Measurement of $\Delta R/R_0$ during cyclic tension was performed up to cycle 2000 (except for the highest stress amplitude of 97% fracture stress, at which fatigue failure occurred at cycle 22) at various stress amplitudes and the results are shown in Table I. The reversible part of $\Delta R/R_0$ increased significantly with increasing stress amplitude, and less significantly with increasing cycle number, as shown in both Table I and Fig. 4. The irreversible part of $\Delta R/R_0$ was much smaller than the reversible part of $\Delta R/R_0$ at the lowest stress amplitude (30% fracture stress), but exceeded the reversible part of $\Delta R/R_0$ at higher stress amplitudes. The irreversible part of $\Delta R/R_0$ increased with stress amplitude much more significantly than the reversible part of $\Delta R/R_0$ for the whole range of stress amplitudes studied. As the stress amplitude was increased beyond 90% of the fracture stress, both the reversible part (Fig. 4) and irreversible part (Fig. 5) of $\Delta R/R_0$ increased abruptly. Both the reversible and irreversible parts of $\Delta R/R_0$ increased with cycle number, but the effect was small compared to the effect of the stress amplitude (Table I, Figs 4 and 5). The reversible strain increased with increasing stress amplitude linearly up to a stress amplitude of 90% of the frature stress and abruptly increased upon further increase of the stress amplitude (Fig. 6). The magnitude of the irreversible strain was much lower than that of the reversible strain at all stress amplitudes (Table I). Both reversible and irreversible strains increased with cycle number, but the effect of both is small compared to the effect of the stress amplitude (Table I).

The secant modulus obtained at the maximum stress decreased with increasing stress amplitude and with increasing cycle number (Table I), but the effect was very small, particularly when the stress amplitude was $\leqslant 70\%$ of the fracture stress. However, as shown in the stress–strain curves obtained during cyclic loading at a stress of 93% of the fracture stress (Fig. 7), the tangent modulus during the first loading (101 GPa) was higher than the secant modulus during first unloading (79 GPa) and subsequent loading and

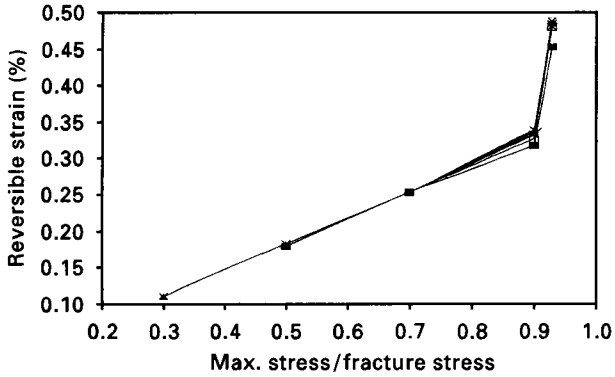

Figure 6 Variation of the reversible strain with stress amplitude (fraction of fracture stress) for various fixed cycle numbers ((■) 1, (□) 20, (✳) 100, (×) 200, (▲) 300 and (⧖) 2000) for a carbon–carbon composite.

unloading (Table I). The stress–strain curves during first unloading and subsequent loading and unloading, essentially overlapped and were not linear. The non-linearity was such that the slope increased with increasing strain; this is attributed to the stretching of the longitudinal woven fibres in the composite. This stretching is expected to occur more easily when the matrix is damaged. The abrupt decrease in tangent modulus during the first loading (Fig. 7) is attributed to damage; it was not observed at lower stress amplitudes, but is consistent with the big jump in the irreversible part of $\Delta R/R_0$ when the stress amplitude changed from 90% to 93% of the fracture stress (Table I).

The reversible part of $\Delta R/R_0$ is mainly due to reversible dimensional changes and correlates with reversible strain. The irreversible part of $\Delta R/R_0$ is due to damage. Although the decreases in irreversible strain and modulus also indicate damage, the changes in these parameters are very small compared to the change in the irreversible part of $\Delta R/R_0$. The great sensitivity of the irreversible part of $\Delta R/R_0$ to damage is also shown by the significant non-zero value of the irreversible part of $\Delta R/R_0$ after merely the first cycle, even at a stress amplitude of just 20% of the fracture stress (Fig. 8). However, the incremental rise in irreversible $\Delta R/R_0$ beyond ~ 500 cycles was small. The composite damage probably involved fibre–matrix interface weakening, matrix cracking and fibre breakage; these origins of damage could not be distinguished through the experimental technique used. Nevertheless, the increase of the irreversible part of $\Delta R/R_0$ as cycling progressed provided a continuous indication of the extent of damage. That the reversible part of $\Delta R/R_0$ also increased with cycling and that an abrupt increase of the irreversible part of $\Delta R/R_0$ is associated with an abrupt increase in the reversible part of $\Delta R/R_0$ (Figs 4 and 5) suggest that the reversible part of $\Delta R/R_0$ is partly associated with a phenomenon which intensifies as damage increases, although it is mostly associated with dimensional changes. This phenomenon may be reversible crack opening during tension, as cracks are expected to increase in size and/or density as cycling progresses. This interpretation is consistent with the observation that an abrupt increase in the reversible part of $\Delta R/R_0$ is associated with an abrupt increase in reversible strain (Figs 4 and 6) and that the abrupt increase in reversible strain occurs at stress amplitudes beyond the range in which the reversible strain is linear in relation to the stress amplitude (Fig. 5).

2.3. Conclusion

A carbon–carbon composite was found to be able to sense its damage and dynamic strain through changes in its d.c. electrical resistance. The resistance increased irreversibly due to damage and increased reversibly upon tensile straining in the elastic regime. The damage sensitivity was so high that even the damage after the first cycle of tensile loading within the elastic regime was detected. The continuous increase in the irreversible $\Delta R/R_0$ as cycling progressed provided continuous monitoring of the extent of fatigue damage, although various extents of damage before cycle ~ 500 could be distinguished more clearly than those after cycle ~ 500. The reversible resistance increase upon reversible straining was mainly due to dimensional changes, but it was partly due to a phenomenon (probably reversible crack opening) that intensified as damage increased.

3. Carbon fibre polymer–matrix composite

In contrast to the continuous carbon fibres in the carbon–carbon composite of Section 2, this section addresses polymer-matrix composites with short randomly oriented carbon fibres. Early fatigue damage was not observed in continuous carbon fibre polymer–matrix composites [16], due to the electrically insulating nature of the polymer matrix making the electrical resistance measurement insensitive to matrix cracks unless the crack cuts across contacting fibres. On the other hand, early fatigue damage was observed in short carbon fibre polymer-matrix composites (this section) due to the matrix damage increasing the chance for adjacent short fibres to touch one another, thereby irreversibly decreasing the resistivity. Thus damage causes the resistivity to decrease for a short carbon fibre polymer-matrix composite, but causes the resistivity to increase for a continuous carbon fibre carbon-matrix composite.

3.1. Experimental procedure

The matrix was polyether sulphone (PES), a thermoplastic of volume resistivity $>10^{10}\,\Omega$cm and provided as Victrex PES 4100P by ICI. The carbon fibres of 10 μm diameter were of length 1 mm and volume resistivity $10^{-3}\,\Omega$cm, and were provided as Carboflex by Ashland Petroleum Co., Ashland, KY. The carbon filaments (to be distinguished from carbon fibres) of 0.15 μm diameter were of length $>100\,\mu$m, as provided as ADNH by Applied Sciences Inc., Cedarville, OH. The carbon filaments had a bent morphology, resembling cotton wool. In contrast, the carbon fibres were straight. In this work, the term "filaments" refers

TABLE I $\Delta R/R_0$, strain gauge factor and modulus obtained during cyclic tension at various stress amplitudes

	Cycle number	Maximum stress (± 1 MPa)					
		114	190	266	342	355	370
Max. stress/fracture stress		0.30	0.50	0.70	0.90	0.93	0.97
$\Delta R/R_0$ (±0.001%)							
Reversible	1	0.185	0.230	0.331	0.442	0.639	0.968
	2	0.173	0.222	–	0.477	0.762	1.090
	20	0.171	0.221	0.335	0.510	0.913	1.203
	100	0.185	0.238	0.360	0.541	1.021	–
	200	0.186	0.251	0.343	0.602	1.030	–
	300	0.185	0.243	0.331	0.622	1.139	–
	2000	0.197	0.243	0.342	0.620	1.204	–
Irreversible	1	0.048	0.220	0.403	0.642	2.632	4.228
	2	0.060	0.228	–	0.729	2.841	4.432
	20	0.062	0.276	0.552	0.938	3.390	5.452
	100	0.073	0.321	0.631	1.220	3.978	–
	200	0.072	0.379	0.690	1.283	4.211	–
	300	0.072	0.402	0.719	1.342	4.253	–
	2000	0.073	0.448	0.748	1.384	4.463	–
Strain (±0.001%)							
Reversible	1	–	0.180	0.256	0.322	0.459	–
	2	–	0.180	0.256	0.329	0.468	–
	20	–	0.180	0.256	0.331	0.486	–
	100	–	0.183	0.256	0.336	0.487	–
	200	0.111	0.184	0.255	0.338	0.490	–
	300	0.111	0.183	0.256	0.341	0.491	–
	2000	0.111	0.184	0.255	0.344	0.494	–
Irreversible	1	–	0.002	0.009	0.000	0.024	–
	2	–	0.002	0.009	0.000	0.024	–
	20	–	0.002	0.009	0.004	0.030	–
	100	–	0.002	0.010	0.007	0.057	–
	200	0.003	0.002	0.010	0.008	0.079	–
	300	0.003	0.002	0.010	0.010	0.090	–
	2000	0.003	0.003	0.015	0.010	0.106	–
Gauge factor (±0.01)							
	1	–	1.28	1.29	1.37	1.39	–
	2	–	1.23	–	1.45	1.63	–
	20	–	1.23	1.31	1.54	1.88	–
	100	–	1.30	1.41	1.61	2.10	–
	200	1.68	1.36	1.35	1.78	2.10	–
	300	1.67	1.33	1.29	1.82	2.32	–
	2000	1.77	1.32	1.34	1.80	2.44	–
$\Delta R/R_0$ due to reversible dimensional change[a] (±0.01%)							
	1	–	0.28	0.39	0.50	0.71	–
	2	–	0.28	0.39	0.51	0.72	–
	20	–	0.28	0.39	0.51	0.75	–
	100	–	0.28	0.39	0.52	0.75	–
	200	0.17	0.28	0.39	0.52	0.76	–
	300	0.17	0.28	0.39	0.53	0.76	–
	2000	0.17	0.28	0.39	0.53	0.76	–
Secant modulus (± 1 GPa)							
	1	–	106	104	106	101[b]79	–
	2	–	106	104	104	77	–
	20	–	106	104	103	74	–
	100	–	104	104	102	74	–
	200	103	103	104	101	74	–
	300	103	104	104	100	74	–
	2000	103	103	104	99	73	–

[a] $\Delta R/R_0$ (%) due to reversible dimensional change was calculated by $\Delta R/R_0 = [(1 + \nu_{12} + \nu_{13})\varepsilon]/[1 - (\nu_{12} + \nu_{13})\varepsilon]$ where ε is the reversible strain. ν_{12} and ν_{13} are the Poisson's ratios. ($\nu_{12} = 0.11$, $\nu_{13} = 0.43$, as separately measured.)
[b] Tangent modulus during the first loading before the abrupt modulus drop.

to fibres of diameter ~0.15 μm and the term "fibres" refers to fibres of diameter ~10 μm.

The composites were fabricated by mixing the polymer powder (100–150 μm size) and the fibres/filaments with water in a blender, drying the wet mix at 120 °C, and subsequent hot pressing in a steel mould at 310 °C (the processing temperature for PES, as recommended by ICI) and 13.4 MPa for ~30 min.

The electrical resistance, R, was measured using the four-probe method while cyclic tension was applied in

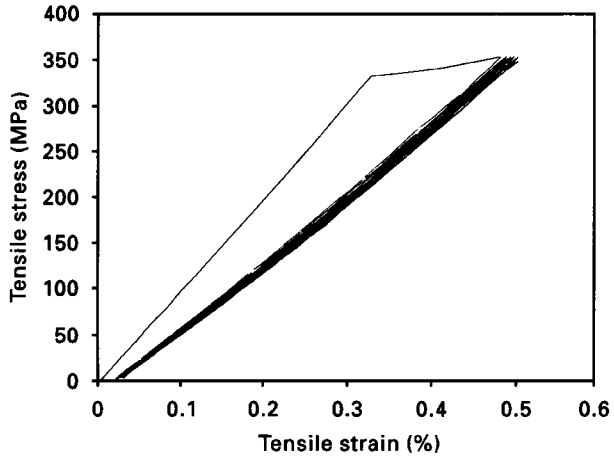

Figure 7 Tensile stress–strain curves obtained during the first 10 cycles at a stress amplitude equal to 93% fracture stress for a carbon–carbon composite.

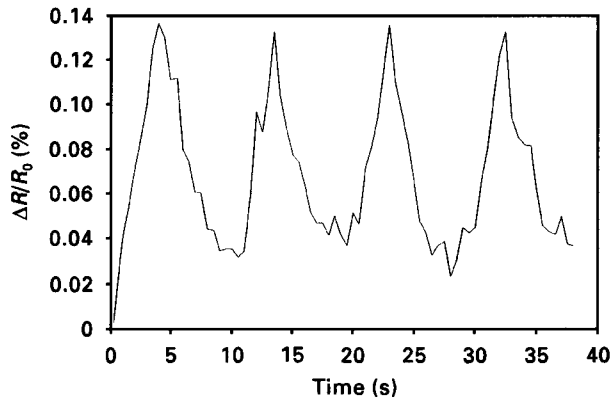

Figure 8 Plot of $\Delta R/R_0$ versus time during the first four cycles at a stress amplitude of 20% of the fracture stress for a carbon–carbon composite.

the load control mode. No precaution was made to prevent buckling during compression. Silver paint was used for electrical contacts. The four probes consist of two outer current probes and two inner voltage probes. The resistance, R, refers to the sample resistance between the inner probes. The distance between the inner probes was 25 mm. The samples were of size 80 mm × 8 × 3 mm. The d.c. resistance was measured along the stress axis. The displacement rate was 1.0 mm min^{-1}. The strain was measured by a strain gauge, which was of a type that could withstand repeated strain up to $> 1\%$ without irreversibly changing its resistance. Testing was conducted by using a hydraulic materials testing system (MTS 810).

3.2. Results and discussion

Fig. 9 shows the strain (Fig. 9a), stress (Fig. 9b) and fractional resistance increase, $\Delta R/R_0$, obtained simultaneously during cyclic tension for a composite with 7 vol % carbon filaments. Because of the small strains involved, $\Delta R/R_0$ is essentially equal to the fractional increase in resistivity. Fig. 10 shows the strain and $\Delta R/R_0$ obtained at a similar strain amplitude for

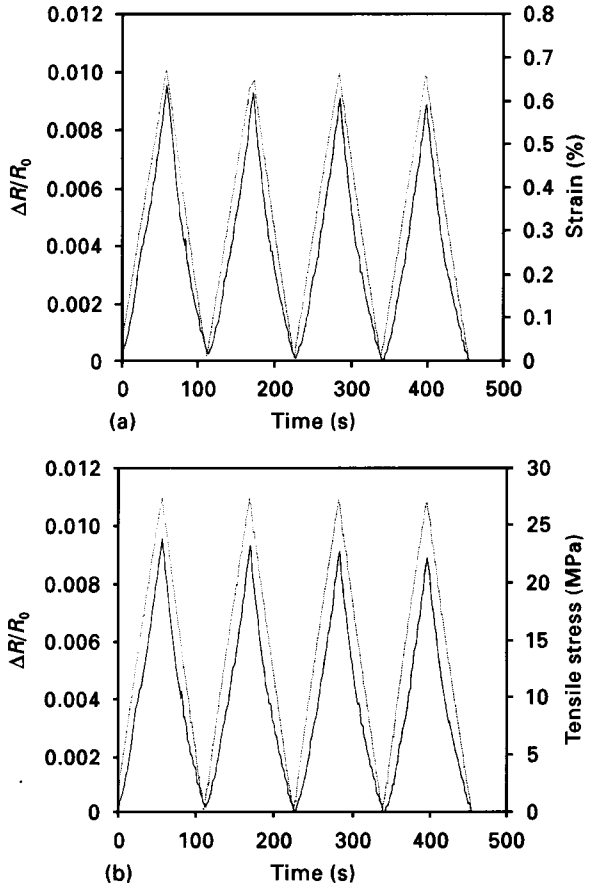

Figure 9 Variation of (——) $\Delta R/R_0$, (– – –) strain (a) and (– – –) stress (b) with time during cyclic tensile loading for a PES-matrix composite containing 7 vol % short carbon filaments.

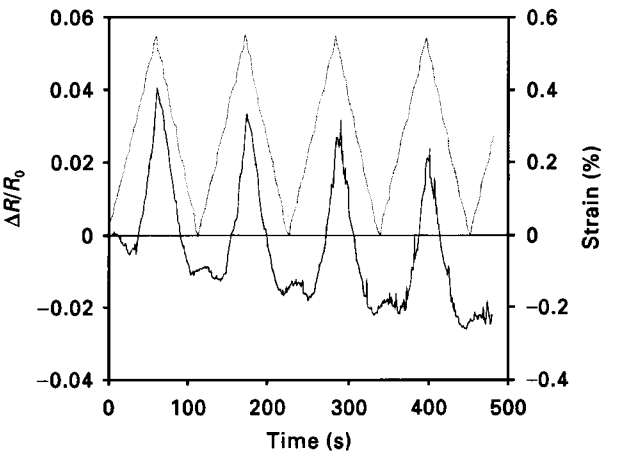

Figure 10 Variation of (——) $\Delta R/R_0$ and (– – –) strain with time during cyclic tensile loading for a PES-matrix composite containing 13 vol % short carbon fibres.

a composite with 13 vol % carbon fibres. (With 7 vol % fibres, the electrical resistivity of the composite was quite high, as shown in Table II, so 13 vol % fibres was used. The percolation threshold was lower for filament composites than fibre composites, as shown by the data in Table II.) The relationship between $\Delta R/R_0$ and strain was far more linear in Fig. 9a than in Fig. 10. In Fig. 10, $\Delta R/R_0$ decreased slightly upon tension, probably due to fibre

TABLE II Volume electrical resistivity of PES-matrix composite with various volume fractions of short carbon filaments and short carbon fibres

Filler (vol %)	Electrical resistivity (Ω cm)	
	Filaments	Fibres
3	112	/
7	3.78	678
13	0.37	16.9
19	0.12	/

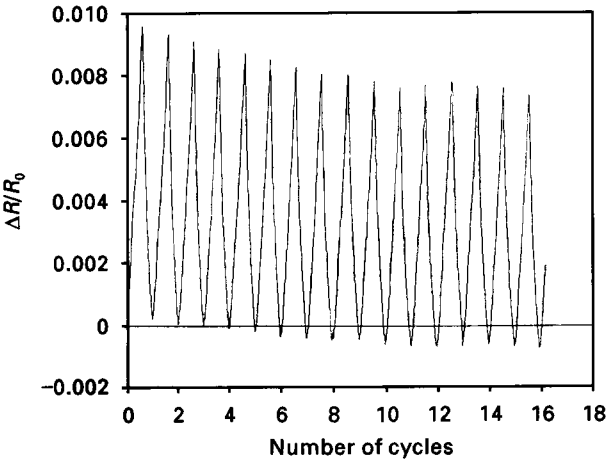

Figure 11 Variation of $\Delta R/R_0$ with cycle number during cyclic tensile loading for a PES-matrix composite containing 7 vol % short carbon filaments (same as Fig. 9 except for more cycles; strain amplitude = 0.7%).

straightening, before abruptly increasing upon further tension due to increase in separation between adjacent fibres; $\Delta R/R_0$ increased slightly toward the end of each cycle (due to fibre buckling) and then decreased at the beginning of the following cycle (due to fibre straightening) before increasing abruptly with increasing strain due to increase in separation between adjacent fibres. In contrast, Fig. 9a does not exhibit this abnormality. Moreover, in Fig. 10, $\Delta R/R_0$ became more and more negative as cycling progressed.

The trend in which $\Delta R/R_0$ became more and more negative as cycling progressed, levelled off after about 10 cycles for both composites, as shown in Fig. 11 for the carbon filament composite of Fig. 9. It is attributed to the decrease in the matrix film thickness at the junction of the filaments or fibres as the cycling progressed (before reaching 10 cycles). A decrease in this thickness led to a decrease in the contact resistivity between the filaments or fibres and thereby a decrease in the volume resistivity of the composite. The extent of decrease was larger for the fibre composite than the filament composite at similar strain amplitudes. This is reasonable because the fibres are more robust than the filaments.

3.3. Conclusion

For both filament and fibre composites, $\Delta R/R_0$ became more negative as cycling progressed up to ~10 cycles, though the effect was more significant for the latter. This effect is probably due to damage in the form of a decrease of the matrix film thickness at the filament–filament or fibre–fibre junction as cycling progressed. After ~10 cycles, $\Delta R/R_0$ does not vary from cycle to cycle.

4. Carbon fibre cement–matrix composite

As in Section 3, this section is concerned with short carbon fibres. However, in contrast to the polymer matrix of Section 3, this section is concerned with the cement matrix. Early fatigue damage was observed in the cement-matrix composite. The effect is similar to that for the polymer-matrix composite; the damage is matrix damage which increases the chance for adjacent fibres to tough one another, thereby decreasing the resistivity irreversibly. Short carbon fibre cement-matrix composites are attractive technologically due to their high flexural strength, high flexural toughness, low drying shrinkage [17–20] and strain-sensing ability [21–23].

4.1. Experimental procedure

The carbon fibres were isotropic pitch-based and unsized, as obtained from Ashland Petroleum Co. (Ashland, KY). The fibre diameter was 10 μm. The nominal fibre length was 5 mm. Fibres in the amount of 0.5% by weight of cement (corresponding to 0.24 vol % mortar) were used. Cement paste made from Portland cement (Type I) from Lafarge Corp. (Southfield, MI) was used for the cementitious material. The water/cement ratio was 0.35. The aggregate used was natural sand, the particle size analysis of which is shown in Fig. 1 of [12]. The sand/cement ratio was 1.0. No large aggregate was used. The water-reducing agent used in the amount of 3% by weight of cement was TAMOL SN (Rohm and Haas Co., Philadelphia, PA), which contained 93%–96% sodium salt of a condensed naphthalenesulphonic acid. Methylcellulose and silica fume were added to help disperse the fibres. Silica fume (no. 965, Elkem Materials Inc., Pittsburgh, PA) was used in the amount of 15% by weight of cement. Methylcellulose (Methocel A15-LV, Dow Chemical Corporation, Midland, MI) in the amount of 0.4% by weight of cement, was used together with a defoamer (Colloids 1010, Colloids Inc., Marietta, GA) in the amount of 0.13 vol %.

Methylcellulose was dissolved in water and then fibres and defoamer were added and stirred by hand for about 2 min. Then this mixture, cement, sand, water, water-reducing agent and silica fume, were mixed in a Hobart mixer for 5 min. The mixer had a flat beater. The slump was 130 mm. After pouring the mix into oiled moulds, a vibrator was used to decrease the amount of air bubbles. The specimens were demoulded after 1 d and then allowed to cure at room temperature in air for 28 d.

Simultaneous to mechanical testing, d.c. electrical resistance measurements were made. For compressive testing, according to ASTM C109-80, specimens were

prepared by using a 2 in. × 2 in. × 2 in. (5.1 cm × 5.1 cm × 5.1 cm) mould. Dog-bone shaped specimens were used for tensile testing. They were prepared by using moulds of the same shape and size. The strain was measured by the crosshead displacement in compressive testing or by a strain gauge in tensile testing, while the fractional change in electrical resistance along the stress axis was measured using the four-probe method. The electrical contacts were made by silver paint. Although the spacing between the contact increased upon tensile deformation and decreased upon compressive deformation, the increase was so small that the measured resistance remained essentially proportional to the resistivity. Testing was performed under cyclic loading (tensile or compressive) at stress amplitudes equal to 0.30, 0.50 and 0.70 of the fracture stress. For compressive testing, a hydraulic mechanical testing system (MTS Model 810) was used, such that each cycle took 38.1 s. For tensile testing, a screw-action mechanical testing system (Sintech 2/D) was used, such that each cycle took 52.2 s.

4.2. Results

Fig. 12 gives the fractional resistance increase, $\Delta R/R_0$, during cyclic compressive loading at a stress amplitude equal to 0.70 of the fracture stress. Fig. 1a gives the variation during the first 21 cycles; Fig. 1b gives the variation during the first ~300 cycles; Fig. 1c gives the variation during the last 11 cycles before fracture at 5263 cycles. $\Delta R/R_0$ decreased during loading and increased during unloading in each cycle. Fig. 1b shows that $\Delta R/R_0$ had a baseline which monotonically decreased as cycling progressed. This decrease occurred up to 306 cycles, at which the baseline became flat. The flat baseline persisted up to a few cycles before fracture. As shown in Fig. 1c, the baseline showed a slight but consistent increase for a few cycles before fracture. At fracture, $\Delta R/R_0$ abruptly and greatly increased.

Fig. 13 shows results similar to Fig. 12, except that Fig. 13 was obtained under tension rather than compression. The results under tension and compression at various stress amplitudes are summarized in Table III. The number of cycles for which the $\Delta R/R_0$ baseline monotonically lowered, increased with increasing stress amplitude and the lowest point of the $\Delta R/R_0$ baseline decreased (i.e. became more negative) with increasing stress amplitude, whether under tension or compression. Obviously, the greater the stress amplitude, the greater the damage.

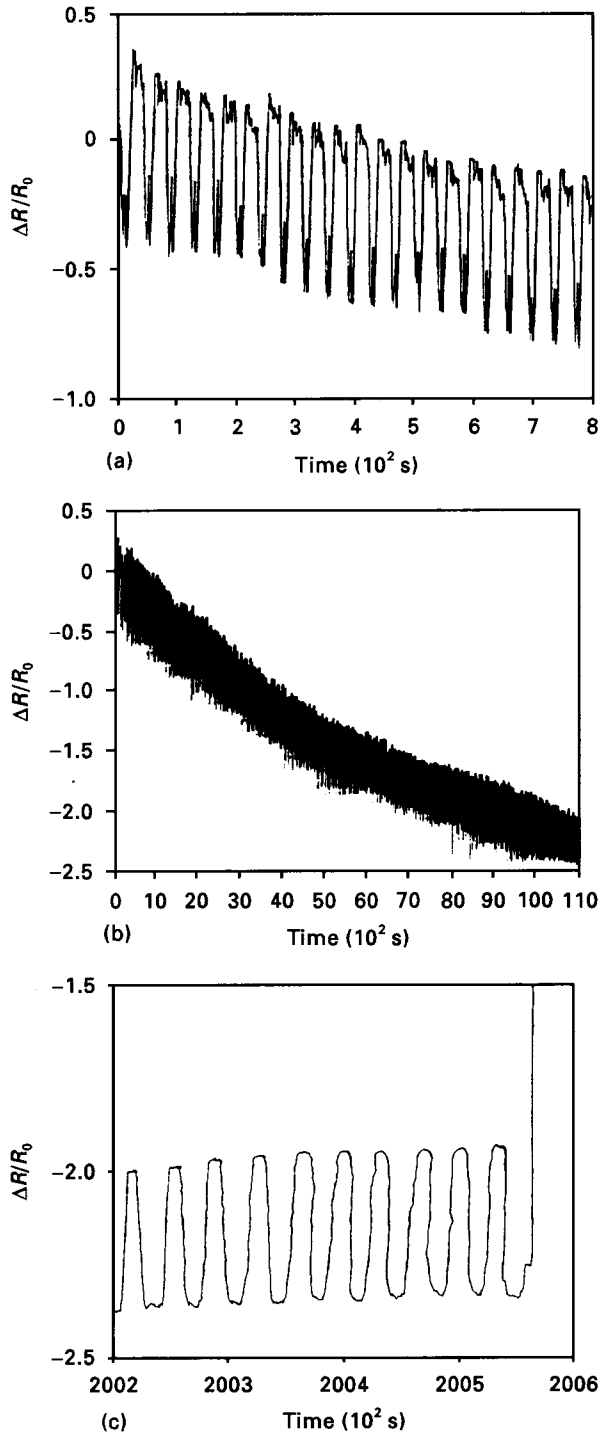

Figure 12 Fractional resistance increase, $\Delta R/R_0$, during cyclic compressive loading of a short carbon fibre cement-matrix composite at a stress amplitude equal to 0.70 fracture stress. (a) First 21 cycles, (b) first ~300 cycles, (c) last 11 cycles before fatigue failure at 5263 cycles.

4.3. Discussion

The $\Delta R/R_0$ baseline monotonically decreased upon cyclic loading from the first cycle up to a cycle number ranging from 123–347 (depending mainly on the stress amplitude). This decrease is attributed to the damage of the cement matrix separating adjacent fibres at their junction. This damage enhanced the chance for adjacent fibres to touch one another, thereby causing the $\Delta R/R_0$ baseline to decrease. It occurred only in the early fatigue life, i.e. 5.8% compressive fatigue life at a stress amplitude of 0.70 fracture stress, or 9.2% tensile fatigue life at a stress amplitude of 0.70 fracture stress. Although the $\Delta R/R_0$ baseline decrease was clear and monotonic, it was not linear with cycle number. Nevertheless, it provides an indication of the extent of early damage.

The damage of the cement matrix between adjacent fibres at their junction occurs upon cyclic loading. This is, at least partly, because reversible (but very slight) fibre pull-out occurs during each strain cycle [22]. After a certain number of cycles, this damage has

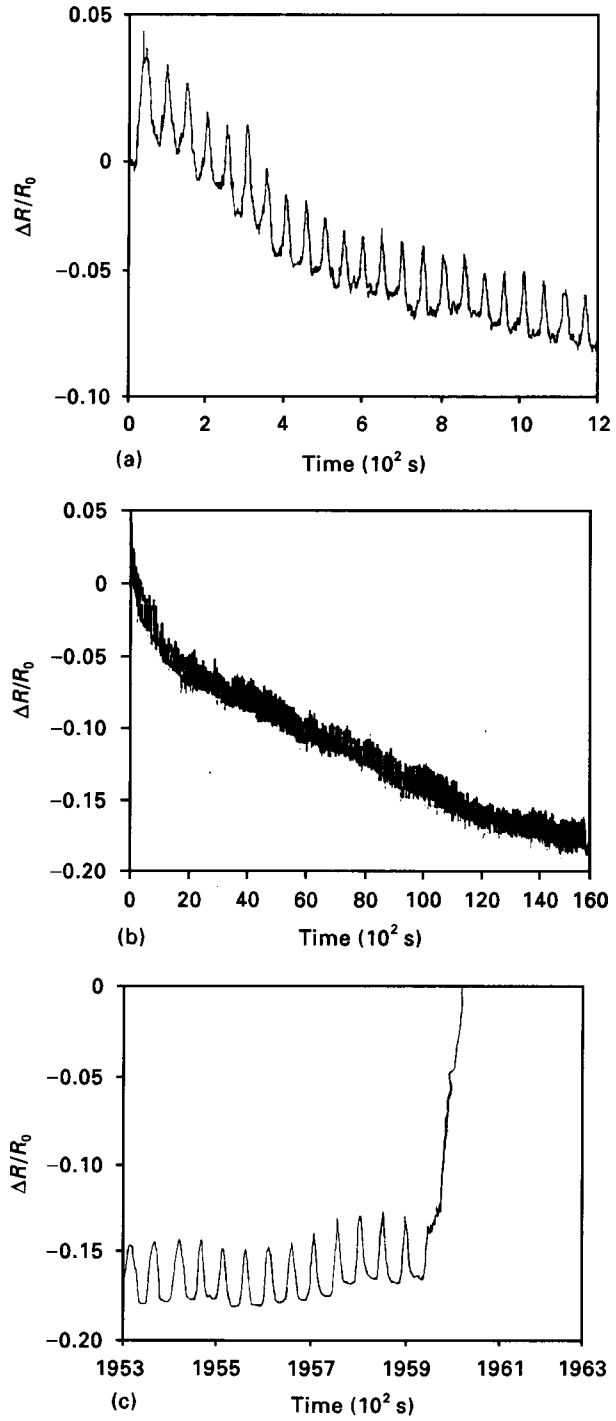

Figure 13 Fractional resistance increase, $\Delta R/R_0$, during cyclic tensile loading of a short carbon fibre cement-matrix composite at a stress amplitude equal to 0.70 fracture stress. (a) First 23 cycles, (b) first ~300 cycles, (c) last 11 cycles before fatigue failure at 3756 cycles.

stabilized, so that there is no further damage of this type upon further cycling. As a result, the $\Delta R/R_0$ baseline decrease occurs only for a limited number of cycles.

4.4. Conclusion

Damage in the early part (<10%) of fatigue life was found to occur in short carbon fibre-reinforced mortar such that the damage resulted in an irreversible decrease (by up to 2%) in the volume electrical resistivity of the mortar. The greater the stress amplitude, the greater the damage, the greater the resistivity decrease and the greater the number of stress cycles for which the resistivity decrease monotonically occurred. The resistivity decrease is attributed to the damage of the cement matrix separating adjacent fibres at their junction.

TABLE III Effect of damage during cyclic loading on the $\Delta R/R_0$ baseline for a short carbon fibre cement-matrix composite

Maximum stress / Fracture stress	Minimum $\Delta R/R_0$	No. of cycles to reach minimum $\Delta R/R_0$
Compression		
0.30	− 0.38	123
0.50	− 1.0	217
0.70	− 2.5	306
Tension		
0.30	− 0.6	146
0.50	− 1.2	252
0.70	− 2.0	347

5. Discussion

Early fatigue refers to damage in the initial portion of the fatigue life. Because early fatigue is most severe in the first cycle, its origin is actually not fatigue but rather damage under static loading. After the first cycle, damage continues to occur but at a diminishing pace. Even at a stress amplitude as low as 20% of the fracture stress, damage occurs after just one loading cycle, as shown for a carbon–carbon composite. Although the origin of early fatigue is not fatigue, early fatigue is expected to contribute to the origin of true fatigue which occurs later in the fatigue life. Although this works shows the occurrence of early fatigue in three kinds of composites, early fatigue is believed to occur in most fibrous composites. This is because the three kinds of composite include composites with brittle and ductile matrices (carbon, cement and thermoplast), those with continuous and short fibres, and those with fibre volume fractions covering a wide range. That early fatigue is not detected does not mean that it does not occur, as the sensitivity of the electrical resistance measurement for damage depends on the structure of the composite. For example, early fatigue was not detected in continuous carbon fibre epoxy-matrix composite by electrical resistance measurement [16] due to the poor sensitivity to damage in an insulating matrix, but it probably occurred. Composites which are totally insulating (both matrix and reinforcement) cannot be analysed at all by d.c electrical resistance measurement. In spite of the limitation of this technique, it is much more sensitive to early damage than acoustic emission.

6. Conclusion

Early fatigue damage (<10% of the fatigue life) was observed in continuous carbon fibre carbon-matrix composite, short carbon fibre polymer-matrix

composite and short carbon fibre cement-matrix composite by d.c. electrical resistance measurement. The damage was most severe in the first loading cycle and the incremental damage in each subsequent cycle diminished cycle by cycle until it approached zero. For the carbon-matrix composite, the resistance increased irreversibly during early fatigue due to matrix damage and possibly fibre fracture as well. For the short fibre polymer-matrix and cement-matrix composites, the resistance decreased irreversibly during early fatigue due to matrix damage near the junction of adjacent fibres, and the resulting increase in the chance that adjacent fibres touched one another.

Acknowledgements

This work was supported in part by National Science Foundation and in part by Defence Advanced Research Projects Agency.

References

1. M. FUWA, B. HARRIS and A. R. BUNSELL, *J. Phys. D Appl. Phys.* **8** (1975) 1460.
2. M. FUWA, A. R. BUNSELL and B. HARRIS, *J. Strain Analy.* **11**(2) (1976) 97.
3. E. U. LEE, D. M. GRANATA and W. R. SCOTT, in "Cyclic Deformation, Fracture, and Non-destructive Evaluation of Advanced Materials", ASTM STP 1157, edited by M. R. Mitchell and O. Buck (American Society for Testing and Materials, Philadelphia, PA, 1992) pp. 293–311.
4. P. P. GROSSKOPF and J. C. DUKE Jr, *ibid.* pp. 278–292.
5. M. FUWA, A. R. BUNSELL and B. HARRIS, *J. Phys. D Appl. Phys.* **9** (1976) 353.
6. *Idem, J. Mater. Sci.* **10** (1975) 2062.
7. R. A. BADCOCK and G. F. FERNANDO, *Smart Mater. Struct.* **4** 1995, 223.
8. K. SCHULTE and Ch. BARON, *Compos. Sci. Technol.* **36** (1989) 63.
9. K. SCHULTE, *J. Phys. IV*, **3** (1993) 1629.
10. R. PRABHAKARAN, *Exp. Techn.* February (1990) 16.
11. O. CEYSSON, M. SALVIA and L. VINCENT, *Scripta Mater.* **34** (1996) 1273.
12. S. WANG and D. D. L. CHUNG, *Carbon* **35** (1997) 621.
13. X. SHUI and D. D. L. CHUNG, *Smart Mater. Struct.* **5** (1996) 243.
14. X. FU and D. D. L. CHUNG, *Cem. Concr. Res.* **26** (1996) 15.
15. X. WANG and D. D. L. CHUNG, *Smart Mater. Struct.* **5** (1996) 796.
16. *Idem, ibid.* **6** (1997) 504.
17. P. CHEN and D. D. L. CHUNG, *Composites* **24** (1993) 33.
18. N. BANTHIA, in "Fibre Reinforced Concrete", SP-142, edited by J. I. Daniel and S. P. Shah (American Concrete Institute, Detroit, IL, 1994) pp. 91–119.
19. P. SOROUSHIAN, F. AOUADI and M. NAGI, *ACI Mater. J.* **88** (1991) 11.
20. S. B. PARK, B. I. LEE and Y. S. LIM, *Cem. Concr. Res.* **21** (1991) 589.
21. P. CHEN and D. D. L. CHUNG, *J. Am. Ceram. Soc.* **78** (1995) 816.
22. D. D. L. CHUNG, *Smart Mater. Struct.* **4** (1995) 59.
23. P. CHEN and D. D. L. CHUNG, *ibid.* **2** (1993) 22.

Received 30 June 1997
and accepted 22 April 1998